Am J Transl Res 2026;18(1):124-139
www.ajtr.org /ISSN:1943-8141/AJTR0170279

Original Article

Inhibiting OAS3 suppresses the development of clear cell renal cell carcinoma by reducing cell proliferation and altering the tumor immune microenvironment

Xinxin Liao, Peng Huang, Haibin Zhou

Department of Urology, Affiliated Hospital of Jiujiang University, Jiujiang 332000, Jiangxi, China

Received November 25, 2025; Accepted December 25, 2025; Epub January 15, 2026; Published January 30, 2026

Abstract: Background: Immune checkpoint inhibitors have been approved for first-line treatment of metastatic clear cell renal cell carcinoma (ccRCC), but limited therapeutic effects have been reported in patients with advanced ccRCC. Investigating vital targets in specific immune interactions and their effect on the tumor microenvironment of ccRCC could provide novel strategies for overcoming the above limitations. Methods: We investigated the expression characteristics, prognostic role, and immune associations of OAS3 in the tumor microenvironment in patients with ccRCC. The functions of OAS3 in proliferation and migration were explored in 786-O and OS-RC-2 cells by forced OAS3 overexpression or knockdown. Furthermore, a xenograft model was established in C57BL/6 mice to study the combined effects of OAS3 downregulation and anti-PD1 therapy. The growth, proliferation, and apoptosis of tumor cells, as well as the infiltration of CD8+ T cells and M1/M2 macrophages within tumor tissues, were evaluated by immunohistochemistry. Results: OAS3 was upregulated in ccRCC and significantly associated with the overall survival of patients with ccRCC. OAS3 expression levels were correlated with genomic mutation profiles and were positively associated with the infiltration of CD8+ T cells, macrophages, neutrophils, and dendritic cells. OAS3 upregulation increased the proliferation, migration, invasion, and colony formation abilities of 786-O and OS-RC-2 cells. In contrast, OAS3 knockdown had the opposite effect. *In vivo* experiments revealed that OAS3 downregulation repressed the growth and proliferation of tumor cells, and promoted infiltration of M2 macrophages but enhanced the apoptosis and infiltration of CD8+ T cells. The phosphorylation of NF-κB p65 was repressed by OAS3 downregulation. In addition, the combination of anti-PD1 therapy and OAS3 downregulation had synergistic antitumor effects. Conclusion: OAS3 is upregulated in ccRCC and promotes tumor progression by mediating the infiltration of immune cells in the TME. OAS3 represents a promising therapeutic target for enhancing the antitumor effects of immune checkpoint inhibitors.

Keywords: OAS3, renal cancer, immune microenvironment, immune checkpoint inhibitor

Introduction

Renal cell carcinoma (RCC) is one of the most common malignant solid tumors of the urinary system. According to statistics, there are approximately 400,000 new cases worldwide each year and approximately 170,000 deaths [1]. In the United States, RCC is the sixth most common cancer in men and ranks ninth in women [1]. Among these, clear cell renal cell carcinoma (ccRCC) is the main pathologic subtype, accounting for 70%-85% of all RCC cases [2]. Approximately 50% of RCC cases are discovered incidentally during physical examination, whereas at the time of diagnosis, approximately 15% of patients present with distant metastasis [3]. The 5-year survival rate for early-stage ccRCC can reach 90%, but once metastasis occurs, the 5-year survival rate is only approximately 12% [4]. Currently, there are various clinical treatment methods for ccRCC, including surgery, radiotherapy, cryotherapy, immunotherapy, local radiotherapy, and targeted therapy for metastasis [5]. Although surgical resection is effective for treating localized low-risk ccRCC, approximately 40% of patients still relapse within a short period after surgery, while those with high-risk or metastatic disease require systemic therapy to improve their prognosis [6, 7]. In recent years, with the wide-

https://doi.org/10.62347/RTZV5102

spread clinical application of targeted therapies and immunotherapies, the overall survival rate of patients has improved. However, owing to individual differences in treatment response and the emergence of drug resistance, most patients eventually progress to advanced ccRCC, for which the 5-year survival rate is less than 10% [8]. Therefore, it is necessary to identify new immune molecular markers to improve the early diagnosis, prognostic evaluation, and personalized treatment of RCC.

The tumor microenvironment (TME) is a complex system composed of multiple components, including tumor cells, immune cells, stromal cells, the extracellular matrix (ECM), blood vessels, soluble factors, and physical properties, and plays critical roles in the processes of tumorigenesis, recurrence, and metastasis [9]. In ccRCC, the TME often exhibits significant immunosuppressive characteristics, which are manifested by the infiltration of regulatory T cells (Tregs), myeloid-derived suppressor cells (MDSCs), and M2-type macrophages; these cells jointly weaken effective antitumor immune responses [10-12]. Notably, ccRCC is one of the most vascularized and immune-infiltrated solid tumors. This provides a basis for its immunotherapeutic use while also constituting a complex background for drug resistance [13]. Differences in the components of the TME can lead to individual variations in responses to immunotherapy, thereby affecting clinical efficacy [14]. Over the past decade, immune checkpoint inhibitors targeting key T-cell regulatory factors, such as PD-1, PD-L1, and CTLA-4, have achieved remarkable progress in the treatment of ccRCC, with significant efficacy by both monotherapy and combination regimens [15, 16]. However, a considerable proportion of patients still experience primary or acquired resistance, leading to no initial response or loss of previously acquired efficacy during treatment, which has become one of the main challenges currently faced in ccRCC immunotherapy [17]. Therefore, elucidating the mechanisms of resistance mediated by the tumor microenvironment in depth and developing effective combination treatment strategies accordingly are crucial for improving the immunotherapeutic outcomes of ccRCC patients and ultimately overcoming the dilemma of resistance.

2’,5’-Oligoadenylate synthetase (OAS) is an interferon (IFN)-induced enzyme that, upon activation by double-stranded RNA, converts ATP into 2’,5’-linked oligoadenylates [18]. The OAS gene family consists of four key members: OAS1, OAS2, OAS3, and OAS-like protein (OASL). In addition to their primary antiviral functions, the OAS gene family is also extensively involved in processes such as apoptosis and growth and is associated with a variety of immune-related diseases [19]. In recent years, OAS3 was shown to play a significant regulatory role in tumors. For example, high OAS3 expression is associated with poor prognosis in breast cancer patients [20]. Studies on pancreatic cancer have identified OAS3 as a key target for reversing antitumor immune resistance, with high OAS3 expression indicating poor prognosis. Targeting OAS3 not only inhibits M2d polarization and the protumor functions of macrophages but also synergistically enhances the effects of chemotherapy and immunotherapy, demonstrating important therapeutic potential [21]. However, in melanoma and clear cell renal cell carcinoma (ccRCC), higher OAS3 expression is associated with better clinical outcomes following immune checkpoint blockade (ICB) therapy [22]. Nevertheless, the specific function of OAS3 in ccRCC and its mechanism in regulating the tumor immune microenvironment remain to be elucidated.

This study aimed to analyze the expression characteristics of OAS3 in ccRCC, its prognostic relevance, and its correlation with immune cell infiltration through bioinformatic methods. Furthermore, *in vitro* and *in vivo* experiments will be conducted to investigate the regulatory effects of OAS3 on ccRCC cell proliferation, migration, invasion, *in vivo* growth, and the immune microenvironment. This study aims to provide new references for the diagnosis of ccRCC and immunotherapy decision-making.

Materials and methods

Bioinformatics analysis

TIMER3 (https://compbio.cn/timer3/) was used to analyze the expression of OAS3 in human cancers and for immune infiltration analysis of OAS3 in KIRC. OAS3 gene and protein expression in KIRC was analyzed via UALCAN (https://ualcan.path.uab.edu/) and GEPIA (http://gepia2.cancer-pku.cn/#index). The Human Protein Atlas (https://www.proteinatlas.org/) was used for analyzing OAS3 expression via IHC detection. The associations of OAS3 levels with the survival of KIRC patients were

determined via the Kaplan-Meier plotter (http://kmplot.com/analysis/). LinkedOmics is an open website that provides multiomics data analysis from all 32 TCGA cancer types. To derive biological insights from the association results, the LinkInterpreter module performs enrichment analysis on the basis of Gene Ontology, biological pathway, and network module data, among other functional categories (https://www.linkedomics.org/login.php).

Cells and cell culture

Two ccRCC cell lines, 786-O (#CL-0010) and OS-RC-2 (CL-0177), were purchased from Procell (Wuhan, China). The culture medium was composed of 89% RPMI-1640, 10% fetal bovine serum (FBS, #26010074, Gibco, California, USA) and 1% penicillin/streptomycin (#15140122, Gibco, California, USA). The cells were incubated in a temperature (37°C) - and humidity (100%)-controlled incubator containing 5% CO_2. The medium was changed every 2 days.

Cell transfection

Two ccRCC cell lines, 786-O and OS-RC-2, were seeded in 24-well plates. Each well contained approximately $1*10^5$ cells. Twenty-four hours later, the cells were transfected with siRNAs targeting OAS3 (si-OAS3#1, si-OAS3#2), pc-DNA3.1-OAS3 overexpression plasmids, and associated negative controls (si-NC or pc-DNA 3.1 vector). These siRNAs were bought from RIBOBIO (Guangzhou, China), and the overexpression plasmids were bought from Abm (Shanghai, China). An electroporation procedure was used to facilitate the transfection of those vectors. The transfection efficiency was validated by RT-qPCR and western blotting. The siRNA sense sequences for OAS3 and IFR2 were as follows: OAS3 (si-OAS3-1: 5'-GGAAGGAGTTCGTAGAGAA-3'; si-OAS3-2: 5'-GTGTCTACTGGACGGTCAACT-3').

RT-PCR

TRIzol reagent (R0016; Beyotime, China) was used to extract total RNA from 786-O and OS-RC-2 cells, which were cultured in 6-well plates (each well contained $1*10^6$ cells). The PrimeScript™ RT Reagent Kit (RR047A, Takara, Dalian, China) was used to synthesize OAS or GAPDH cDNA. The amplification of the OAS3 gene was carried out via the Premix Ex Taq™ II (RR820A, Takara) Kit. The $2^{-\Delta\Delta Ct}$ method was used to calculate the relative OAS3 expression. GAPDH was used as the internal control. The primers used for OAS3 and GAPDH (Tsingke Biotechnology Co., Ltd., China) were as follows: OAS3 (forward: 5'-TGATCAAGGTGGTCAAGGGTG-3' and reverse: 5'-TGCTCAGTGAACTGGCTGAA-3'); and GAPDH (forward: 5'-ATGGCAAATTCCATGGCACC-3' and reverse: 5'-AGCATCGCCCCACTTGATTT-3').

Western blot

Following cell transfection, total protein was extracted from the ccRCC cell lines 786-O and OS-RC-2. RIPA (#J63306. AP, Thermo Fisher, USA) was used for cell lysis. The total protein concentration was determined by the BCA method (#A55860, Thermo Fisher, USA). Total protein was separated by 10% SDS-PAGE and then transferred onto PVDF membranes. After being blocked with 5% BSA (#AM2616, Thermo Fisher, USA), the membranes were incubated with OAS3 rabbit pAb (#A9481, ABclonal, Wuhan, China) or β-actin (#AC026, ABclonal, Wuhan, China). The incubation temperature was set at 4°C. Fifteen hours later, the membranes were washed with TBST 3 times and then incubated with the secondary antibody goat anti-rabbit IgG H&L (HRP) (#AB6721, Abcam) for 60 min at room temperature. The protein bands were visualized by an enhanced chemiluminescence (ECL) kit (#P0018S, Beyotime, Shanghai, China).

CCK8 assay

786-O and OS-RC-2 cells were seeded in 96-well plates after transfection. Each well contained 2000 cells. The Cell Counting Kit-8 (CCK-8) assay was used to determine cell proliferation. Ten microliters of CCK-8 solution (#C0038, Beyotime, China) was added to each well at 24 h, 48 h, or 72 h after cell seeding. The absorbance was measured at 450 nm to assess the proliferation of the above cells.

Transwell assay

Transwell chambers (Transwell® 8.0 μm, #3422, Corning, USA) were used to measure cell migration and invasion. 786-O and OS-RC-2 cells in the well growth state were collected and resuspended in non-FBS medium. 786-O

and OS-RC-2 cells (5×10^4 cells) in 200 μl of medium were seeded in the upper chambers of Transwells, while the lower chambers were supplemented with 800 μL of medium containing 20% FBS. The cells on the bottom surface were fixed with 100% methanol and stained with 0.5% crystal violet. For the invasion assay, the Transwell chambers were coated with Matrigel (Sigma-Aldrich, St. Louis, MO, USA), and the other procedures were the same in the migration assay. The number of migrated cells was calculated by ImageJ.

Colony formation assay

786-0 and OS-RC-2 cells cultured in 6-well plates (1.5×10^3 cells in each well) were incubated for 14 days. The medium was changed every 3 days. Finally, the cells were washed with PBS twice and fixed with 100% methanol for 15 min. A 0.1% crystal violet solution was used for cell staining. The number of cell colonies (with more than 50 cells) was counted.

EdU staining assay

The proliferation of 786-0 and OS-RC-2 cells following cell transfection was determined using an EdU-staining kit (#40276ES60, YEASEN, Shanghai, China). The above cells were seeded into 24-well platelets. The cell density was adjusted to 6×10^5 cells per well. Twenty-four hours later, 50 μM EdU solution was added to each well, and the cells were incubated at 37°C for 2 h. The cells were fixed with 4% formaldehyde. Nuclei were stained with DAPI solution (#40728ES03, YEASEN, Shanghai, China). The results were subsequently visualized via a fluorescence microscope. The ratio of EdU-positive cells was calculated to evaluate cell proliferation.

Animal studies in mice

All animal experiments were approved by the Ethics Committee of Affiliated Hospital of Jiujiang University. 6-week-old C57BL/6 male mice were purchased from Beijing Vital River Laboratory Animal Technology Co., Ltd. (Beijing, China). A total of 3×10^6 mouse renal cancer cells (RENCA) were suspended in 100 μl of PBS. Before surgery, the mice received 5% isoflurane inhalation to relieve pain. They were then subcutaneously injected into the left flanks of the mice, which were randomly divided into four groups. Two weeks later, the mice were intraperitoneally injected with an anti-PD-1 antibody (3 mg/kg, BE0273, Bio X Cell, West Lebanon, NH, USA) [23]. Tumor sizes were measured every 3 days. Four weeks after cell injection, the mice were sacrificed, and the tumors were removed for histopathologic analysis. The tumor weight was recorded, and the volume was estimated with the following formula: $1/2*(\text{length} \times \text{width}^2)$. In addition, extreme values (maximum and minimum) were eliminated. Euthanasia was performed using 5% isoflurane inhalation followed by cervical dislocation.

Immunohistochemistry

The tumor tissues were fixed in formalin, embedded in paraffin, and sectioned for immunohistochemical staining to detect the expression of Ki-67, CD45, CD163, CD8, Granzyme B, and PD-1. The sections were then incubated with specific primary antibodies against CD45 (1:200, A23549, ABclonal, Wuhan, China), Ki-67 (1:400, A26755PM, ABclonal, Wuhan, China), CD163 (1:200, A8383, ABclonal, Wuhan, China), CD8 (A11856, ABclonal, Wuhan, China), Granzyme B (1:400, A2557, ABclonal, Wuhan, China), and PD-1 (1:200, AF7695, Beyotime, Shanghai, China), followed by incubation with secondary antibodies (A0308, Beyotime, China) conjugated with HRP and DAB for color development.

Immunofluorescence

The tumor sections were prepared and blocked with 5% BSA for 60 min at room temperature. The sections were incubated with an anti-p-p65 antibody (1:200, AP1458, ABclonal, Wuhan, China) at 4°C overnight and with secondary antibodies at 37°C for 1 h. The sections were counterstained with DAPI for 10 min to stain the nuclei. The fluorescence was imaged under a microscope (IX73, Olympus, Japan).

Statistical analysis

GraphPad Prism 10.2 software was used for the statistical analyses (GraphPad, La Jolla, CA, USA). Each group had at least three repetitions. The measured data are presented as the means ± SD. One-way analysis of variance (ANOVA) or two-tailed Student's t test was used to compare quantitative data. *P* values for each analysis are marked in the figures, and the levels of statistical significance were defined as

P<0.05 (**P*<0.05; ***P*<0.01; ****P*<0.001; *****P*<0.0001).

Results

OAS3 mRNA and protein expression is increased in KIRC

The expression of OAS3 in human cancers was analyzed by TIMER3 (https://compbio.cn/timer3/). The OAS3 gene level was increased in most cancers, including KIRC (**Figure 1A**, **1B**). OAS3 gene and protein expression in KIRC was analyzed via UALCAN (https://ualcan.path.uab.edu/). The results revealed that the OAS3 mRNA level was increased in KIRC tissues with increased disease stage (**Figure 1C**) and nodal metastasis (**Figure 1D**). At the protein level, OAS3 expression was also greater in KIRC tissues than in normal tissues (**Figure 1E**, **1F**). The Human Protein Atlas (https://www.proteinatlas.org/) was used to analyze OAS3 expression in tumor tissues through IHC detection. OAS3 was positively expressed in both normal renal tissues and tumor tissues and was located mainly in the cytoplasm and cell membrane (**Figure 1G**).

Association of OAS3 levels with the survival of patients with KIRC

By analyzing OAS3 alterations with respect to the survival of KIRC patients using Kaplan-Meier plotter (http://kmplot.com/analysis/), we found that a higher OAS3 level was associated with good overall survival in KIRC patients (P=0.02, **Figure 2A**). In addition, a higher OAS3 level seemed to be associated with poorer relapse-free survival (P=0.21, **Figure 2B**). We conducted further analysis on the basis of sex and immune cell enrichment. Among male KIRC patients, higher OAS3 could predict poorer OS. In contrast, higher OAS3 in female KIRC patients was associated with better OS (**Figure 2C**). For patients with enriched immune cells, such as CD4+ memory T cells, CD8+ T cells, Tregs, and macrophages, higher OAS3 levels were associated with poorer OS, whereas a decreased immune cell enrichment could reverse this phenomenon (**Figure 2C-G**).

Mechanisms of OAS3 in ccRCC

LinkedOmics was used to analyze possible mechanisms of OAS3 in ccRCC. The top 50 genes with positive or negative associations are shown in **Figure 3A**, **3B**. The enrichment analysis of the LinkInterpreter module revealed that OAS3 was significantly associated with several biologic processes, such as the adaptive immune response, the immune response-regulating signaling pathway, and positive regulation of cytokine production (**Figure 3C**). The KEGG pathways included Th1 cell differentiation, Th1 and Th2 cell differentiation, cell adhesion molecules, and the NF-kappa B signaling pathway (**Figure 3D**, **3E**).

Association of OAS3 with immune cell infiltration in ccRCC

Based on TIMER3 analysis, we found that OAS3 was significantly associated with the infiltration of immune cells (including CD4+ T cells, CD8+ T cells, macrophages, CTL cells, and Th1/Th2 cells) in multiple cancers (**Figure 4A**). In KIRC, OAS3 was positively associated with B cells, CD8+ T cells, CD4+ T cells, neutrophils, and dendritic cells (**Figure 4B**). The SCNA module of TIMER provides a comparison of tumor infiltration levels among tumors with different somatic copy number alterations for a given gene. We did not identify significant associations between OAS3 copy number and the infiltration levels of immune cells (**Figure 4C**).

OAS3 upregulation enhances the proliferation, migration, and invasion of ccRCC cells

An OAS3-overexpressing cell model was constructed in 786-O and OS-RC-2 cells. RT-PCR and WB confirmed the cell transfection efficiency (**Figure 5A**, **5B**). Next, CCK8, colony formation, and EdU staining assays were performed. The results revealed that following OAS3 upregulation, the proliferation and colony formation ability of these two cell lines increased (**Figure 5C-H**). Transwell assays revealed that more migrative and invasive cells in the OAS3-OE group compared to the vector group (**Figure 5I**, **5J**).

Downregulating OAS3 led to reduced proliferation, migration, and invasion of ccRCC cells

To further confirm the roles of OAS3 in ccRCC cell proliferation and migration, we established an OAS3-downregulated cell model (**Figure 6A**, **6B**). Functional assays were then performed. Compared with the si-NC group, the si-OAS3

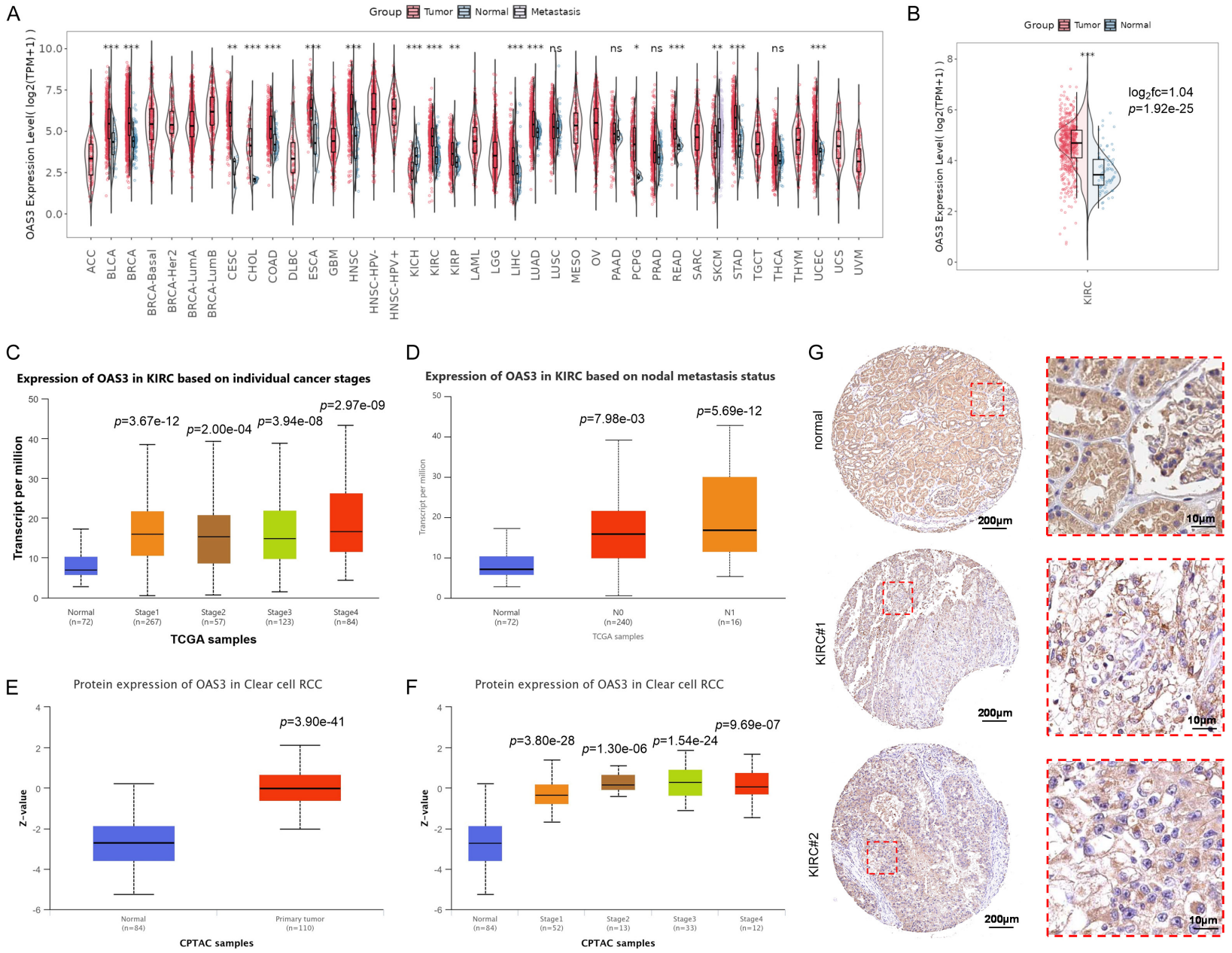
A
Group Tumor Normal Metastasis
OAS3 Expression Level(log2(TPM+1))
ACC BLCA BRCA BRCA-Basal BRCA-Her2 BRCA-LumA BRCA-LumB CESC CHOL COAD DLBC ESCA GBM HNSC HNSC-HPV- HNSC-HPV+ KICH KIRC KIRP LAML LGG LIHC LUAD LUSC MESO OV PAAD PCPG PRAD READ SARC SKCM STAD TGCT THCA THYM UCEC UCS UVM
B
Group Tumor Normal
OAS3 Expression Level(log2(TPM+1))
log2fc=1.04
p=1.92e-25
KIRC
C
Expression of OAS3 in KIRC based on individual cancer stages
Transcript per million
p=3.67e-12
p=2.00e-04
p=3.94e-08
p=2.97e-09
Normal (n=72)
Stage1 (n=267)
Stage2 (n=57)
Stage3 (n=123)
Stage4 (n=84)
TCGA samples
D
Expression of OAS3 in KIRC based on nodal metastasis status
Transcript per million
p=7.98e-03
p=5.69e-12
Normal (n=72)
N0 (n=240)
N1 (n=16)
TCGA samples
E
Protein expression of OAS3 in Clear cell RCC
Z-value
p=3.90e-41
Normal (n=84)
Primary tumor (n=110)
CPTAC samples
F
Protein expression of OAS3 in Clear cell RCC
Z-value
p=3.80e-28
p=1.30e-06
p=1.54e-24
p=9.69e-07
Normal (n=84)
Stage1 (n=52)
Stage2 (n=13)
Stage3 (n=33)
Stage4 (n=12)
CPTAC samples
G
normal
KIRC#1
KIRC#2
200μm
10μm

Figure 1. Expression characteristics of OAS3 mRNA and protein in KIRC. A. The expression of OAS3 in human cancers was analyzed by TIMER3 (https://compbio.cn/timer3/). B. The scatter plot shows the expression of OAS3 in kidney renal clear cell carcinoma (KIRC). C, D. OAS3 gene expression in KIRC was analyzed by UALCAN (https://ualcan.path.uab.edu/). E, F. OAS3 protein expression in KIRC was analyzed by UALCAN. G. The protein level of OAS3 in normal tissue and KIRC tissues was analyzed by the Human Protein Atlas (https://www.proteinatlas.org/).

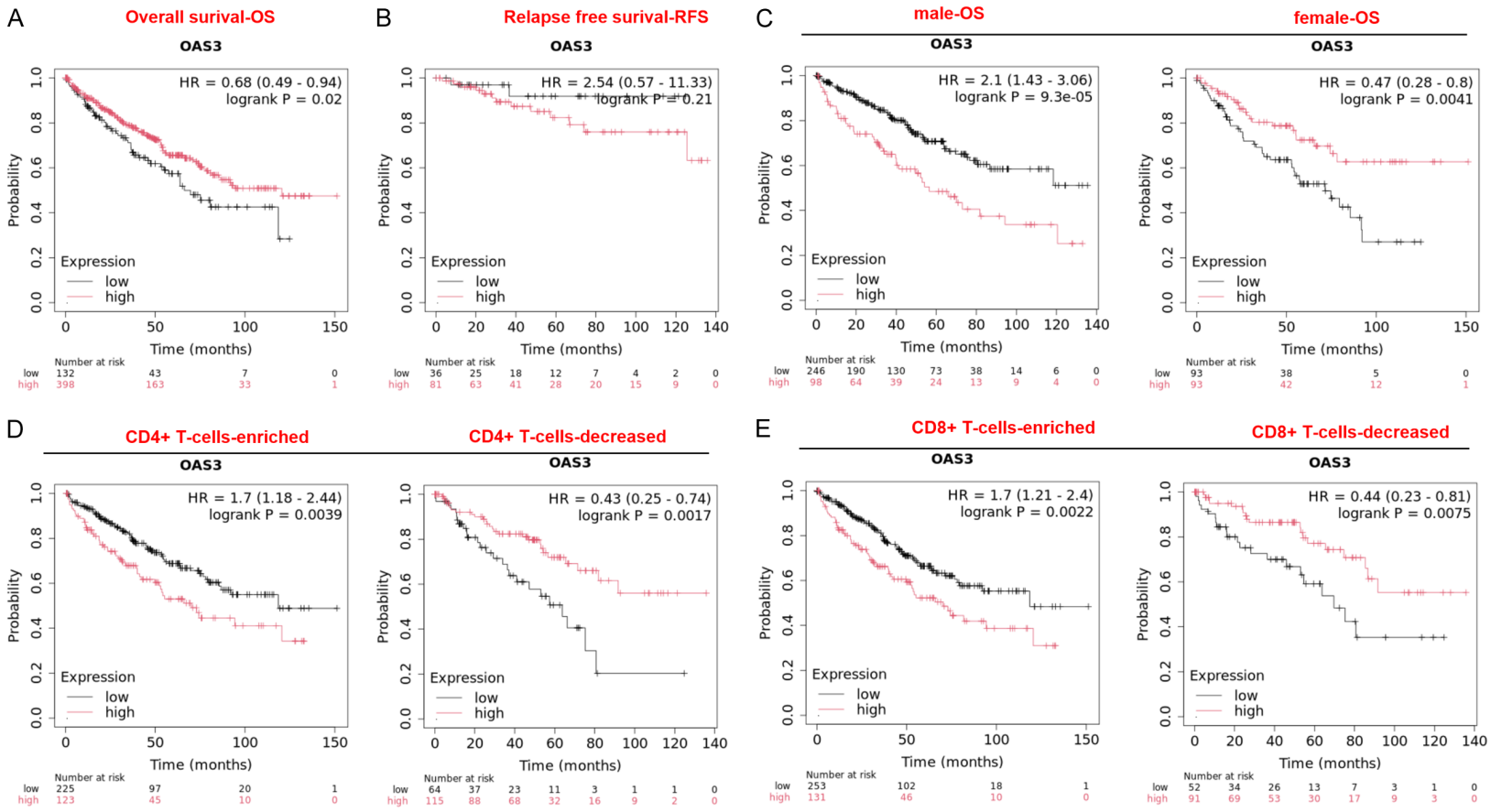

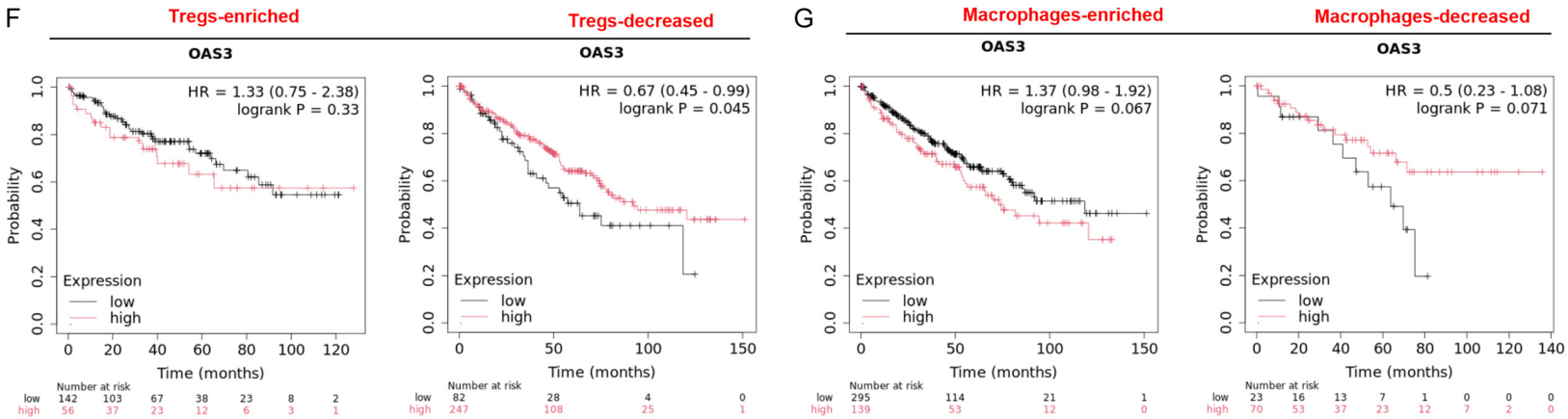

Figure 2. Association of OAS3 levels with the survival of patients with KIRC. The Kaplan-Meier plotter (http://kmplot.com/analysis/) was used for survival analysis. A, B. Associations of OAS3 levels with overall survival (OS) and relapse-free survival (RFS) in KIRC patients. C-G. KIRC patients were divided into subgroups on the basis of sex and immune cell enrichment level.

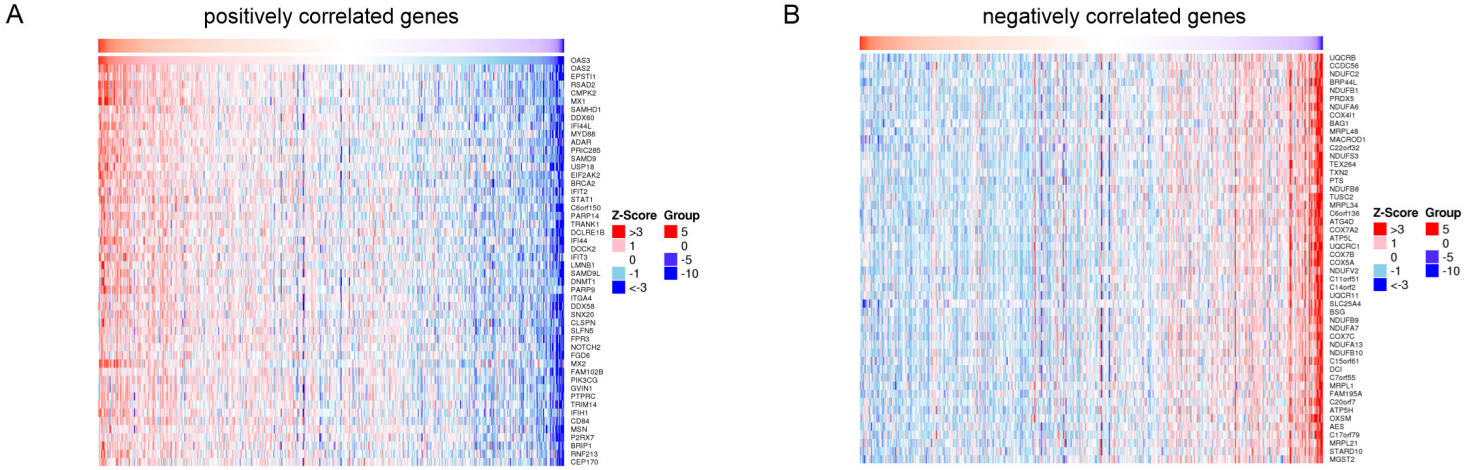

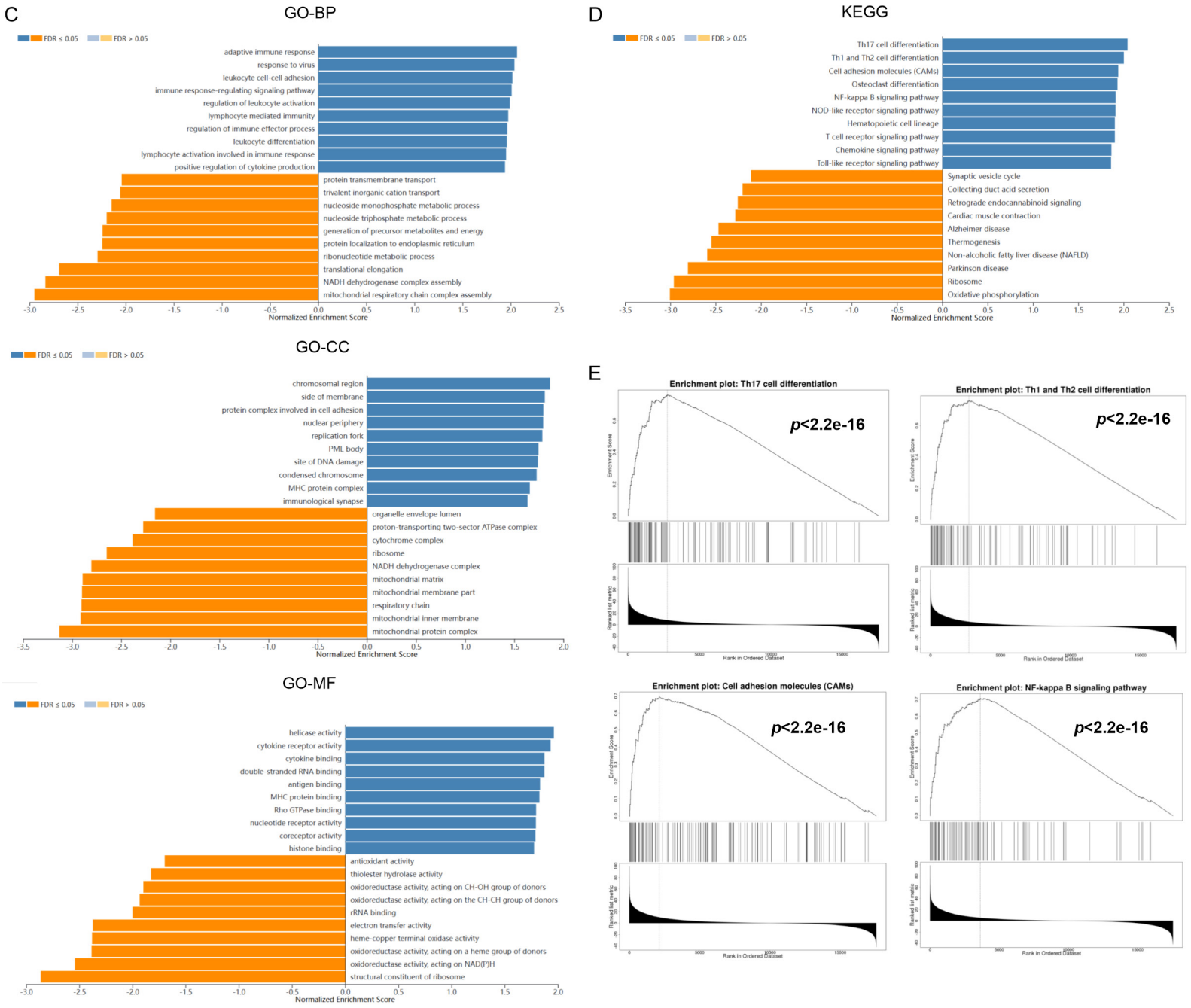
C
GO-BP
FDR ≤ 0.05
FDR > 0.05
adaptive immune response
response to virus
leukocyte cell-cell adhesion
immune response-regulating signaling pathway
regulation of leukocyte activation
lymphocyte mediated immunity
regulation of immune effector process
leukocyte differentiation
lymphocyte activation involved in immune response
positive regulation of cytokine production
protein transmembrane transport
trivalent inorganic cation transport
nucleoside monophosphate metabolic process
nucleoside triphosphate metabolic process
generation of precursor metabolites and energy
protein localization to endoplasmic reticulum
ribonucleotide metabolic process
translational elongation
NADH dehydrogenase complex assembly
mitochondrial respiratory chain complex assembly
Normalized Enrichment Score
GO-CC
chromosomal region
side of membrane
protein complex involved in cell adhesion
nuclear periphery
replication fork
PML body
site of DNA damage
condensed chromosome
MHC protein complex
immunological synapse
organelle envelope lumen
proton-transporting two-sector ATPase complex
cytochrome complex
ribosome
NADH dehydrogenase complex
mitochondrial matrix
mitochondrial membrane part
respiratory chain
mitochondrial inner membrane
mitochondrial protein complex
GO-MF
helicase activity
cytokine receptor activity
cytokine binding
double-stranded RNA binding
antigen binding
MHC protein binding
Rho GTPase binding
nucleotide receptor activity
coreceptor activity
histone binding
antioxidant activity
thiolester hydrolase activity
oxidoreductase activity, acting on CH-OH group of donors
oxidoreductase activity, acting on the CH-CH group of donors
rRNA binding
electron transfer activity
heme-copper terminal oxidase activity
oxidoreductase activity, acting on a heme group of donors
oxidoreductase activity, acting on NAD(P)H
structural constituent of ribosome
D
KEGG
Th17 cell differentiation
Th1 and Th2 cell differentiation
Cell adhesion molecules (CAMs)
Osteoclast differentiation
NF-kappa B signaling pathway
NOD-like receptor signaling pathway
Hematopoietic cell lineage
T cell receptor signaling pathway
Chemokine signaling pathway
Toll-like receptor signaling pathway
Synaptic vesicle cycle
Collecting duct acid secretion
Retrograde endocannabinoid signaling
Cardiac muscle contraction
Alzheimer disease
Thermogenesis
Non-alcoholic fatty liver disease (NAFLD)
Parkinson disease
Ribosome
Oxidative phosphorylation
E
Enrichment plot: Th17 cell differentiation
p<2.2e-16
Enrichment plot: Th1 and Th2 cell differentiation
p<2.2e-16
Enrichment plot: Cell adhesion molecules (CAMs)
p<2.2e-16
Enrichment plot: NF-kappa B signaling pathway
p<2.2e-16

Figure 3. Mechanisms of OAS3 in ccRCC. LinkedOmics was used to analyze for mechanisms of OAS3 in ccRCC. (A, B) The heatmaps how the top 50 genes with positive or negative associations. (C, D) The LinkInterpreter module was used to perform enrichment analysis, and the enriched GO terms, including biological process (BP), cellular component (CC), and molecular function (MF), are shown in (C). (D, E) The enriched KEGG pathways included Th1 cell differentiation, Th1 and Th2 cell differentiation, cell adhesion molecules, and the NF-kappa B signaling pathway.

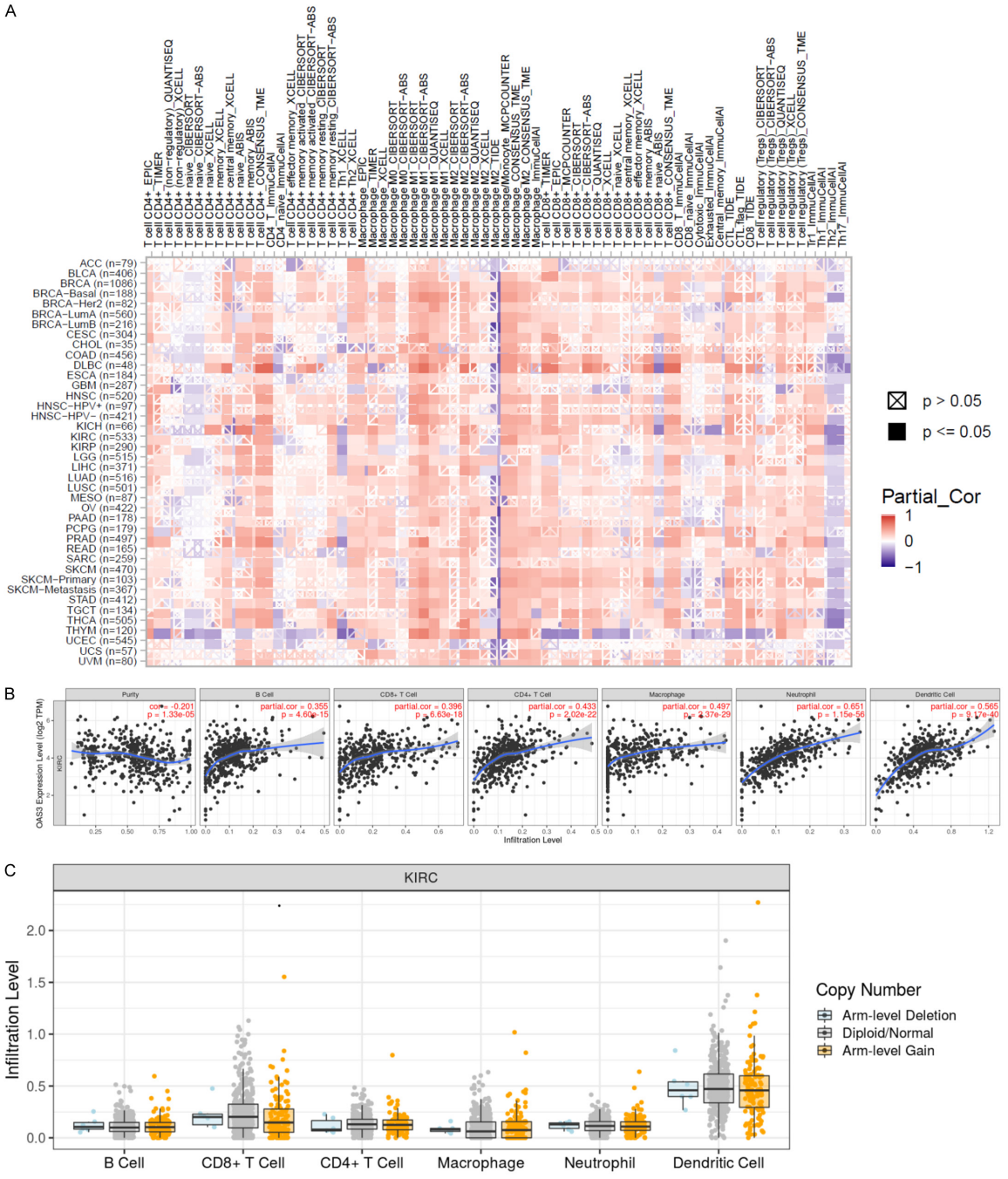

Figure 4. Association of OAS3 with immune cell infiltration in ccRCC. A. TIMER3 was used for analysis of OAS3 expression and the infiltration of immune cells (including CD4+ T cells, CD8+ T cells, macrophages, CTL cells, and Th1/Th2 cells) in multiple cancers. B. OAS3 was positively associated with B cells, CD8+ T cells, CD4+ T cells, neutrophils, and dendritic cells. C. The SCNA module of OAS3 clear cell renal cell carcinoma.

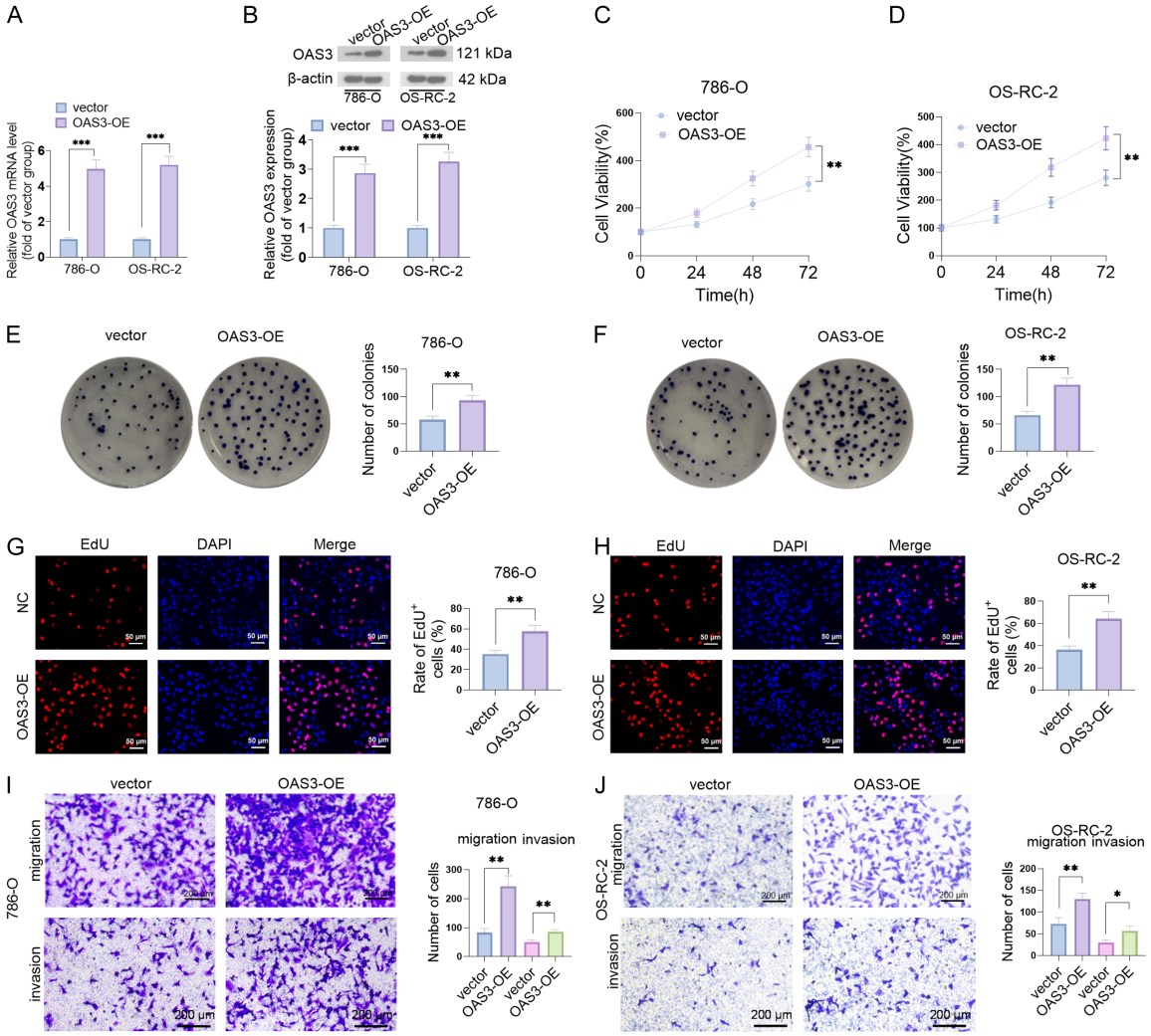

Figure 5. Effects of OAS3 upregulation on the proliferation, migration, and invasion of ccRCC cells. An OAS3-overexpressing cell model was constructed in 786-O and OS-RC-2 cells. A, B. RT-PCR and WB were conducted to measure OAS3 mRNA and protein levels, respectively. C, D. CCK8 assay for assessing cell proliferation. E, F. A colony formation assay was used to determine cell proliferation. G, H. An EdU staining assay was performed to test cell proliferation. I, J. Cell migration and invasion were was tested using the Transwell assay. Scale bar =200 μm. The data are presented as the means ± SDs. n=3. * indicates P<0.05, ** indicates P<0.01, *** indicates P<0.001.

group exhibited reduced cell proliferation, migration, and invasion (**Figure 6C-J**). We conducted *in vivo* experiments on C57BL/6 mice. Compared with those in the si-NC group, the tumor volume and weight in the si-OAS3 group were significantly lower (**Figure 7A-C**). Ki67 and TUNEL staining suggested that downregulation of OAS3 reduced cell proliferation and enhanced apoptosis (**Figure 7D**, **7E**).

Downregulation of OAS3 enhances the antitumor effects of anti-PD-1 therapy

We treated the tumor-bearing mice with an anti-PD-1 antibody. The results revealed that the tumor volume and weight were decreased by anti-PD-1 therapy (**Figure 7A-C**). Compared to the anti-PD-1 group, the anti-PD-1+si-OAS3 group presented further reductions in tumor volume and weight (**Figure 7A-C**). Moreover, anti-PD-1 therapy attenuated the percentage of KI67-positive cells while increasing the percentage of TUNEL-positive cells. Downregulation of OAS3 further enhanced the effects mediated by anti-PD-1 (**Figure 7D**, **7E**). We then conducted IHC to analyze the infiltration of immune cells in the tumors. We found that anti-PD-1 therapy increased the number of CD45-, CD8-, and granzyme B-positive cells while reducing CD163 and PD-1 expression.

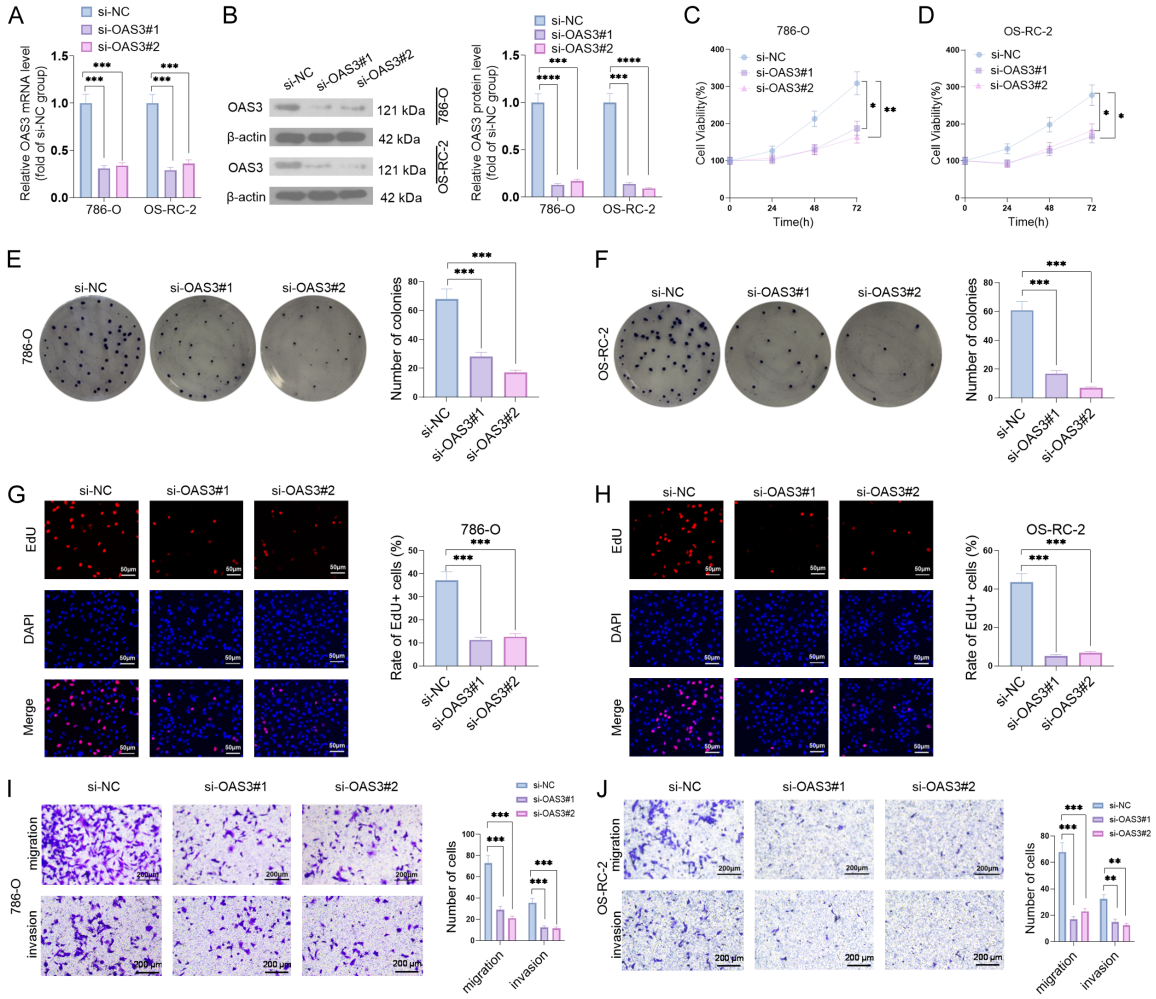

Figure 6. Effects of OAS downregulation on the proliferation migration, and invasion of ccRCC cells. An OAS3 downregulation cell model was constructed in 786-O and OS-RC-2 cells. A, B. RT-PCR and WB were conducted to measure OAS3 mRNA and protein levels, respectively. C, D. CCK8 assay for examining cell proliferation. E, F. A colony formation assay was used to measure alterations in cell proliferation. G, H. An EdU staining assay was performed to test cell proliferation. Scale bar =50 μm. I, J. Cell migration and invasion were tested using the Transwell assay. Scale bar =200 μm. The data are presented as the means ± SDs. n=3. * indicates P<0.05, ** indicates P<0.01, *** indicates P<0.001, **** indicates P<0.0001.

Moreover, combining anti-PD-1 and si-OAS3 further promoted these alterations through anti-PD-1 therapy (**Figure 7F-J**). Considering that OAS3 potentially affects the NF-κB pathway in ccRCC, we analyzed the associations between OAS3 levels and PDL1 or NFκB1 expression. The results revealed a positive association (**Figure 7K**, **7L**). IF was conducted to measure p-p65 in the tumor tissues. Anti-PD-1 therapy or downregulating OAS3 can decrease p-p65 levels. Combining anti-PD-1 and si-OAS3 further reduced p-p65 expression (**Figure 7M**).

Discussion

The programmed cell death protein 1 (PD-1) pathway has drawn significant interest because of its involvement in triggering the immune checkpoint response in T cells, enabling tumor cells to escape immune surveillance and often making them highly resistant to standard chemotherapy. The use of anti-PD-1/PD-L1 antibodies as checkpoint inhibitors is quickly emerging as a promising strategy for cancer treatment. Nonetheless, not all patients experience complete responses, and adverse events

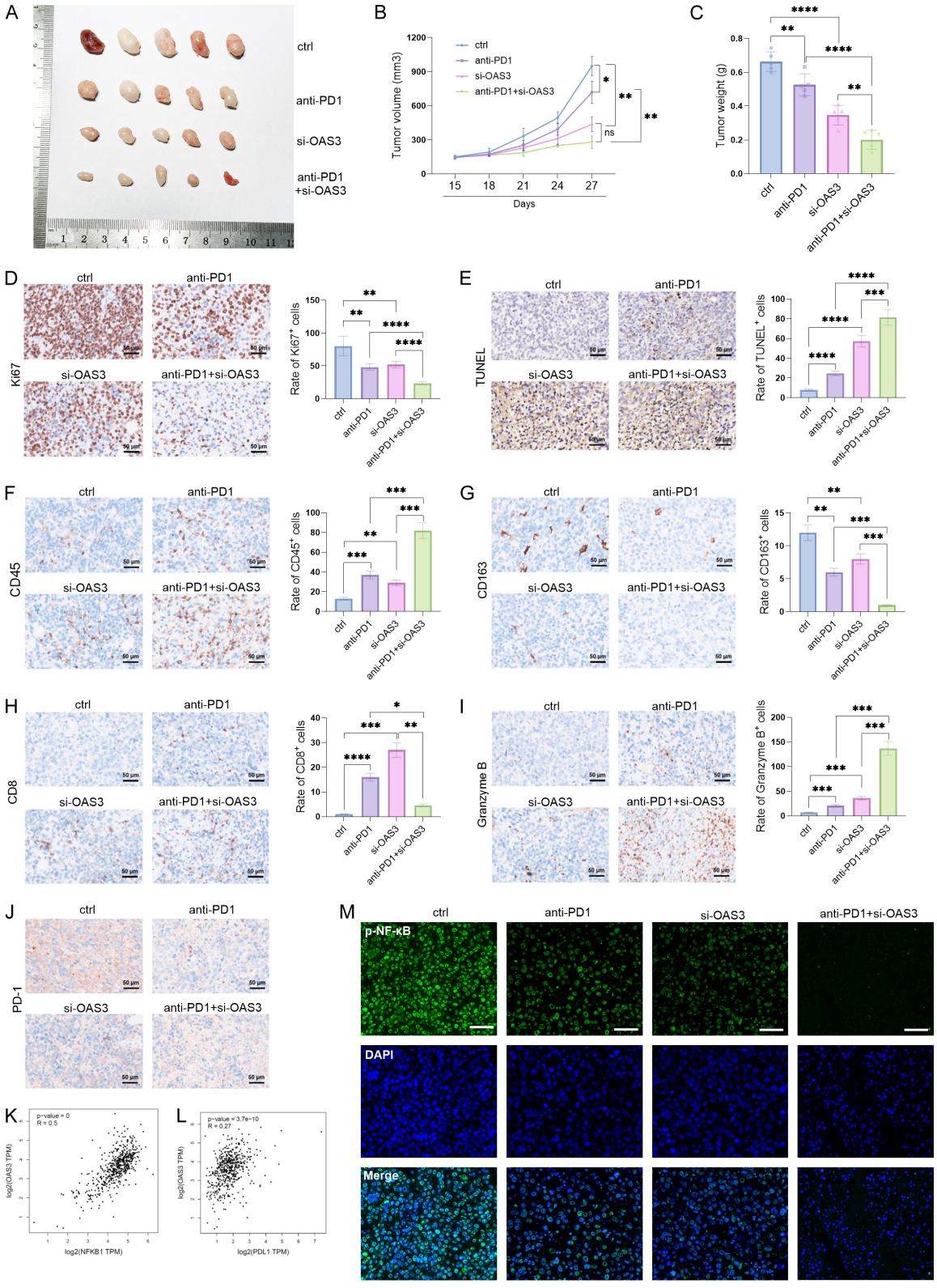

Figure 7. Effects of downregulating OAS3 and anti-PD-1 therapy on cell growth and the immune microenvironment. The RENCA mouse renal cancer cells were transfected with si-NC or si-OAS3 and then used for the *in vivo* study. Tumor-bearing mice were treated with anti-PD-1 (3 mg/kg). A. Images of the tumors. B, C. The tumor volume and weight were calculated. D-J. IHC was conducted to detect Ki67, TUNEL, CD45, CD8, PD-1, CD163, and granzyme B expression in the tumor tissues. Scale bar =50 μm. K, L. The associations between OAS3 levels and PDL1 or NFκB1

expression were analyzed via GEPIA. M. IF was conducted to measure p-p65 expression in the tumor tissues. Scale bar =50 μm. The data are presented as the means ± SDs. n=5. * indicates P<0.05, ** indicates P<0.01, *** indicates P<0.001, **** indicates P<0.0001.

have been reported [24, 25]. In this study, we investigated the role of OAS3 in ccRCC progression. We found that OAS3 is upregulated in ccRCC and is closely associated with patient survival. We further performed a functional assay and reported that OAS3 upregulation increased cell proliferation, migration, and invasion, whereas OAS3 downregulation had the opposite effect. Moreover, the combination of anti-PD-1 therapy and OAS3 downregulation resulted in enhanced antitumor effects, suggesting that targeting OAS3 is a strategy to overcome anti-PD-1 resistance.

OAS3 has been found to be a diagnostic biomarker in human cancers. For example, increased OAS3 is positively correlated with advanced cancer stage and poor overall survival in patients with breast cancer and gastric cancer [26, 27]. In bladder cancer, Gao et al. reported that OAS3 expression was elevated in tumor tissues compared to normal tissues. However, a higher OAS3 level was associated with better patient survival [28]. In this study, we found that higher OAS3 levels predicted better OS, but not RFS in ccRCC patients. Interestingly, the predictive roles of OAS3 in ccRCC differed significantly according to sex and immune cell infiltration status. Higher OAS3 levels predicted poorer OS in male ccRCC patients, whereas female ccRCC patients had better OS with higher OAS3 expression. In general, the incidence of ccRCC is twice as high in males as in females worldwide, and the prognosis is also worse in males. Biological sex may be an important predictor, and sex-specific tailored treatment may improve patient care in patients with ccRCC [29]. Our data also suggest that OAS3 is a sex-related gene involved in ccRCC development.

OAS3 is regarded as a potential modulator in the immune microenvironment of cancers [21]. Elevated OAS3 expression might promote the infiltration of CD4+ T cells, CD8+ T cells, neutrophils, and dendritic cells in the microenvironment of bladder cancer [28]. In this study, we found that OAS3 downregulation repressed the proliferation and growth of ccRCC cells. Combining anti-PD-1 therapy with OAS3 downregulation further reduced tumor volume and weight by disrupting proliferation and enhancing apoptosis. OAS3 downregulation increased the number of CD45-, CD8-, and granzyme B-positive cells while reducing CD163 and PD-1 expression. Moreover, combining anti-PD-1 and si-OAS3 further promoted these alterations through anti-PD-1 therapy. Therefore, these studies suggest that targeting OAS3 can induce antitumor effects by modulating the immune microenvironment of ccRCC.

The NF-κB pathway plays multiple essential roles in the cancer immune microenvironment, one of which is modulating the functions of tumor-associated macrophages [30]. Targeting this pathway may reverse the immunosuppressive microenvironment [31]. Persistent NF-κB activation in tumor cells or stromal cells upregulates the expression of immunosuppressive molecules such as PD-L1, IDO1, and TGF-β. It also promotes the recruitment and activation of Tregs, myeloid-derived suppressor cells (MDSCs), and M2-type tumor-associated macrophages (TAMs), creating a barrier that inhibits antitumor immune cell infiltration and function [32-35]. Constitutive NF-κB activation - often caused by mutations in upstream regulators such as NIK, IKKα/β, or the loss of IκBα - directly upregulates PD-L1 transcription. This leads to excessive PD-L1 expression on tumor cells, overriding the blocking effect of anti-PD-1 antibodies and reestablishing T-cell exhaustion [36]. Therefore, combining NF-κB inhibitors with anti-PD-1 therapy has shown synergistic effects in preclinical models, highlighting the potential of this combinatorial approach to improve patient outcomes. Here, we found that OAS3 positively regulates the NF-κB pathway. In ccRCC, there are positive associations between OAS3 levels and PDL1 or NFκB1. Both anti-PD-1 therapy and downregulating OAS3 can decrease p-p65 levels, and combining anti-PD-1 therapy with si-OAS3 further reduces p-p65 expression. Therefore, knocking down OAS3 might promote the antitumor effects of anti-PD-1 through repressing the NF-κB pathway.

Several limitations remain in this study. First, the expression characteristics of OAS3 need to be confirmed in clinical samples. Considering

that OAS3 predicts the OS of ccRCC patients in a sex-dependent manner, it would be interesting to pay special attention to OAS3 expression in different sexes. Second, the downstream mechanism, including the NF-κB pathway of OAS3, should be further investigated.

Conclusion

Our bioinformatic analysis data suggested that OAS3 expression is upregulated in ccRCC. OAS3 downregulation inhibited ccRCC cell proliferation, migration, and invasion, and enhanced the efficacy of anti-PD-1 therapy. OAS3 was closely associated with immune cell infiltration in the tumor microenvironment. Downregulation of OAS3 reduced the infiltration of "M2" macrophages and enhanced the infiltration of CD8+ T cells, potentially by mediating the PD-1 and NF-κB pathways. We propose and validate a novel strategy to increase antitumor immunity by downregulating OAS3, offering a clinically actionable avenue to improve ccRCC therapy.

Disclosure of conflict of interest

None.

Address correspondence to: Haibin Zhou, Department of Urology, Affiliated Hospital of Jiujiang University, No. 57 Xunyang East Road, Xunyang District, Jiujiang 332000, Jiangxi, China. Tel: +86-07922180180; E-mail: doczhou@126.com

References

[1] Siegel RL, Miller KD, Wagle NS and Jemal A. Cancer statistics, 2023. CA Cancer J Clin 2023; 73: 17-48.
[2] Rose TL and Kim WY. Renal cell carcinoma: a review. JAMA 2024; 332: 1001-1010.
[3] Siegel RL, Giaquinto AN and Jemal A. Cancer statistics, 2024. CA Cancer J Clin 2024; 74: 12-49.
[4] Siegel RL, Miller KD and Jemal A. Cancer statistics, 2015. CA Cancer J Clin 2015; 65: 5-29.
[5] Abah MO, Ogenyi DO, Zhilenkova AV, Essogmo FE, Ngaha Tchawe YS, Uchendu IK, Pascal AM, Nikitina NM, Rusanov AS, Sanikovich VD, Pirogova YN, Boroda A, Moiseeva AV and Sekacheva MI. Innovative therapies targeting drug-resistant biomarkers in metastatic clear cell renal cell carcinoma (ccRCC). Int J Mol Sci 2024; 26: 265.
[6] Ingels A, Campi R, Capitanio U, Amparore D, Bertolo R, Carbonara U, Erdem S, Kara Ö, Klatte T, Kriegmair MC, Marchioni M, Mir MC, Ouzaïd I, Pavan N, Pecoraro A, Roussel E and de la Taille A. Complementary roles of surgery and systemic treatment in clear cell renal cell carcinoma. Nat Rev Urol 2022; 19: 391-418.
[7] Larroquette M, Peyraud F, Domblides C, Lefort F, Bernhard JC, Ravaud A and Gross-Goupil M. Adjuvant therapy in renal cell carcinoma: Current knowledges and future perspectives. Cancer Treat Rev 2021; 97: 102207.
[8] Ge Q, Meng J, Wang Z, Anwaier A, Lu J, Tian X, Wang Y, Yang J, Zhang H, Ye D and Xu W. Spatially segregated APOE+ macrophages restrict immunotherapy efficacy in clear cell renal cell carcinoma. Theranostics 2025; 15: 5312-5336.
[9] Fu T, Dai LJ, Wu SY, Xiao Y, Ma D, Jiang YZ and Shao ZM. The spatial architecture of the immune microenvironment orchestrates tumor immunity and the therapeutic response. J Hematol Oncol 2021; 14: 98.
[10] Kim MC, Borcherding N, Ahmed KK, Voigt AP, Vishwakarma A, Kolb R, Kluz PN, Pandey G, De U, Drashansky T, Helm EY, Zhang X, Gibson-Corley KN, Klesney-Tait J, Zhu Y, Lu J, Lu J, Huang X, Xiang H, Cheng J, Wang D, Wang Z, Tang J, Hu J, Wang Z, Liu H, Li M, Zhuang H, Avram D, Zhou D, Bacher R, Zheng SG, Wu X, Zakharia Y and Zhang W. CD177 modulates the function and homeostasis of tumor-infiltrating regulatory T cells. Nat Commun 2021; 12: 5764.
[11] Tian J, Cheng C, Gao J, Fu G, Xu Z, Chen X, Wu Y and Jin B. POLD1 as a prognostic biomarker correlated with cell proliferation and immune infiltration in clear cell renal cell carcinoma. Int J Mol Sci 2023; 24: 6849.
[12] Obradovic A, Chowdhury N, Haake SM, Ager C, Wang V, Vlahos L, Guo XV, Aggen DH, Rathmell WK, Jonasch E, Johnson JE, Roth M, Beckermann KE, Rini BI, McKiernan J, Califano A and Drake CG. Single-cell protein activity analysis identifies recurrence-associated renal tumor macrophages. Cell 2021; 184: 2988-3005, e16.
[13] Sjöberg E. Molecular mechanisms and clinical relevance of endothelial cell cross-talk in clear cell renal cell carcinoma. Ups J Med Sci 2024; 129.
[14] Shi N, Chen S, Wang D, Wu T, Zhang N, Chen M and Ding X. MDK promotes M2 macrophage polarization to remodel the tumor microenvironment in clear cell renal cell carcinoma. Sci Rep 2024; 14: 18254.
[15] Wilky BA. Immune checkpoint inhibitors: the linchpins of modern immunotherapy. Immunol Rev 2019; 290: 6-23.
[16] Xu W, Atkins MB and McDermott DF. Checkpoint inhibitor immunotherapy in kidney cancer. Nat Rev Urol 2020; 17: 137-150.

[17] Ballesteros PÁ, Chamorro J, Román-Gil MS, Pozas J, Gómez Dos Santos V, Granados ÁR, Grande E, Alonso-Gordoa T and Molina-Cerrillo J. Molecular mechanisms of resistance to immunotherapy and antiangiogenic treatments in clear cell renal cell carcinoma. Cancers (Basel) 2021; 13: 5981.

[18] Hovnanian A, Rebouillat D, Mattei MG, Levy ER, Marié I, Monaco AP and Hovanessian AG. The human 2',5'-oligoadenylate synthetase locus is composed of three distinct genes clustered on chromosome 12q24.2 encoding the 100-, 69-, and 40-kDa forms. Genomics 1998; 52: 267-77.

[19] Huang YZ, Zheng YX, Zhou Y, Xu F, Cui YZ, Chen XY, Wang ZY, Yan BX, Zheng M and Man XY. OAS1, OAS2, and OAS3 Contribute to Epidermal Keratinocyte Proliferation by Regulating Cell Cycle and Augmenting IFN-1-Induced Jak1-Signal Transducer and Activator of Transcription 1 Phosphorylation in Psoriasis. J Invest Dermatol 2022; 142: 2635-2645, e9.

[20] Zhang Y and Yu C. Prognostic characterization of OAS1/OAS2/OAS3/OASL in breast cancer. BMC Cancer 2020; 20: 575.

[21] Zhang S, Xu X, Zhang K, Lei C, Xu Y, Zhang P, Zhang Y, Gu H, Huang C and Qiu Z. Targeting OAS3 for reversing M2d infiltration and restoring anti-tumor immunity in pancreatic cancer. Cancer Immunol Immunother 2024; 74: 37.

[22] Li XY, Hou L, Zhang LY, Zhang L, Wang D, Wang Z, Wen MZ and Yang XT. OAS3 is a co-immune biomarker associated with tumor microenvironment, disease staging, prognosis, and treatment response in multiple cancer types. Front Cell Dev Biol 2022; 10: 815480.

[23] Zhang B, Wang CM, Wu HX, Wang F, Chai YY, Hu Y, Wang BJ, Yu Z, Xia RH, Xu RH and Cao XT. MFSD2A potentiates gastric cancer response to anti-PD-1 immunotherapy by reprogramming the tumor microenvironment to activate T cell response. Cancer Commun (Lond) 2023; 43: 1097-1116.

[24] Massari F, Santoni M, Ciccarese C, Santini D, Alfieri S, Martignoni G, Brunelli M, Piva F, Berardi R, Montironi R, Porta C, Cascinu S and Tortora G. PD-1 blockade therapy in renal cell carcinoma: current studies and future promises. Cancer Treat Rev 2015; 41: 114-21.

[25] Han L, Meng Y and Jianguo Z. Research progress of PD 1/PD L1 inhibitors in the treatment of urological tumors. Curr Cancer Drug Targets 2024; 24: 1104-1115.

[26] Lu J, Yang L, Yang X, Chen B and Liu Z. Investigating the clinical significance of OAS family genes in breast cancer: an in vitro and in silico study. Hereditas 2024; 161: 50.

[27] Zhang M, Xie J, Yao S, Cai T, Yuan L, Liu X and Wang F. The expression signature, prognostic significance and immune cell infiltration of the OAS gene family in gastric cancer. Sci Rep 2025; 15: 39682.

[28] Gao L, Ren R, Shen J, Hou J, Ning J, Feng Y, Wang M, Wu L, Sun Y, Wang H, Wang D and Cao J. Values of OAS gene family in the expression signature, immune cell infiltration and prognosis of human bladder cancer. BMC Cancer 2022; 22: 1016.

[29] Hwang J, Lee HE, Han JS, Choi MH, Hong SH, Kim SW, Yang JH, Park U, Jung ES and Choi YJ. Sex-specific survival gene mutations are discovered as clinical predictors of clear cell renal cell carcinoma. Sci Rep 2024; 14: 15800.

[30] He R, He Y, Du R, Liu C, Chen Z, Zeng A and Song L. Revisiting of TAMs in tumor immune microenvironment: Insight from NF-κB signaling pathway. Biomed Pharmacother 2023; 165: 115090.

[31] de la Calle-Fabregat C, Calafell-Segura J, Gardet M, Dunsmore G, Mulder K, Ciudad L, Silvin A, Moreno-Càceres J, Corbí ÁL, Muñoz-Pinedo C, Michels J, Gouy S, Dutertre CA, Rodríguez-Ubreva J, Ginhoux F and Ballestar E. NF-κB and TET2 promote macrophage reprogramming in hypoxia that overrides the immunosuppressive effects of the tumor microenvironment. Sci Adv 2024; 10: eadq5226.

[32] Antonangeli F, Natalini A, Garassino MC, Sica A, Santoni A and Di Rosa F. Regulation of PD-L1 Expression by NF-κB in Cancer. Front Immunol 2020; 11: 584626.

[33] Hong Y, Fu Y and Long Q. Posttranslational governance of NF-κB in cancer immunity: mechanisms and therapeutic horizons. Front Immunol 2025; 16: 1627084.

[34] Liu M, Wei F, Wang J, Yu W, Shen M, Liu T, Zhang D, Wang Y, Ren X and Sun Q. Myeloid-derived suppressor cells regulate the immunosuppressive functions of PD-1^{-}PD-L1^{+} Bregs through PD-L1/PI3K/AKT/NF-κB axis in breast cancer. Cell Death Dis 2021; 12: 465.

[35] Mazi FA, Cakiroglu E, Uysal M, Kalyoncu M, Demirci D, Sozeri PYG, Yilmaz GO, Ozhan SE and Senturk S. The paracaspase MALT1 is a downstream target of Smad3 and potentiates the crosstalk between TGF-β and NFκB1 signaling pathways in cancer cells. Cell Signal 2023; 105: 110611.

[36] Cao J, Hu D, Yu H, Xie Y, Mi L, Ye Y, Deng M, Zhang W, Li M, Wang D, Qi F, Wu J, Song Y, Zhu J and Ding N. Interleukin-2-inducible T-cell kinase inhibition to block NF-κB signaling exerts anti-tumor effects and enhances chemotherapy in NK/T-cell lymphoma. Cancer Lett 2025; 618: 217602.